

Research on the direction estimation algorithm of vector hydrophones under near-field and Far-field Reflecting Boundary

Zhenzhen Shang^{1,*}, Xiaoyong Zhang¹, Hairong Kou¹, Libo Yang¹, and Guojun Zhang²

¹ Intelligent Sensing and Multidimensional Information Processing Laboratory, Taiyuan University, Taiyuan, 030032, PR China

² State Key Laboratory of Dynamic Testing Technology, North University of China, Taiyuan, 030051, PR China

Received: 4 March 2025 / Accepted: 7 November 2025

Abstract. To address the impact of reflection boundaries and port and starboard ambiguity on passive sonar positioning, a method of vector hydrophone hybrid source positioning under different reflection boundaries is proposed. When the reflection boundary is close to or located within the near-field Fresnel zone, the reflected waves will increase and decrease because of the superposition of the line-of-sight waves, thus affecting the positioning results. The composite vector hydrophone consists of three-dimensional orthogonal vector channels and scalar channels. By fully utilizing the vector information in the MUSIC algorithm array flow pattern, the ambiguity problem of the azimuth angles on both sides under far-field and near-field reflection boundary conditions can be solved. By establishing different reflection models, the array manifold matrix of the three-dimensional directional angle and distance of the sound source under dual reflection is derived to illustrate the influence of reflection boundaries on position estimation. Comparing the simulation results with Cramer Rao bound (CRB) and maximum likelihood estimation algorithms, it is proven that the proposed method is correct and efficient. Finally, the effectiveness of the method is verified through lake experiments. This study has important guiding significance for the practical promotion of underwater acoustic engineering.

Keywords: Azimuth ambiguity / vector MEMS hydrophone / reflecting boundary / far and near field sources / MUSIC algorithm / signal array manifold

1 Introduction

With the development of ocean acoustics, research on the ocean is increasingly deepening. The ocean acoustic field contains scalar and vector information, and vector hydrophones can synchronously detect scalar pressure and vector data of u ocean sound fields [1,2], which is superior to scalar hydrophones [3], and has highly sensitivity and broadband low-frequency detection performance. Cilia vector MEMS hydrophone, which utilizes piezoresistance and biomimetic principles [4–6] has been used for low-frequency underwater acoustic detection and localization research. In fact, there are always sound boundaries in the process of sound propagation, including underwater boundaries such as the sea surface, seabed, hull, and any obstacles in the water [7,8]. The influence of near-field or far-field reflection boundaries on positioning cannot be ignored. Therefore, high-precision positioning in complex environments has become one of the current research hotspots.

The research on direction angle of arrival estimation (DOA) is relatively mature when the hydrophone is located in far-field source and not close to any boundary. Nehorai and Hawkes studied far-field array manifolds with reflective boundaries and derived CRBs for azimuth and elevation angle [9]. Keshavarz studied the spatial matched filtering pattern of hydrophones located nearby the reflection boundaries [10]. Ahmadi studied the minimum variance estimation method in direction finding near/not near reflection boundaries [11]. Wu et al. derived the near-field array manifold relationship and derived the CRB for angle and range [12–14]. The traditional MUSIC algorithm [15] and beamforming algorithm [16] are used to achieve far-field target orientation. In the near-field Fresnel zone, distance parameters cannot be ignored, and the 2D-MUSIC technology [17] can realize the estimation of angle and range. In more complex far and near field source scenarios, some hybrid sources methods draw on the design of subarrays, which also leads to more complex computational complexity [18,19]. Recently, Shang et al. proposed two hybrid field source MUSIC search algorithms based on vector hydrophone arrays, which can achieve parameter separation of hybrid field sources with less computation

* Corresponding author: shangzhenzhen@tyu.edu.cn

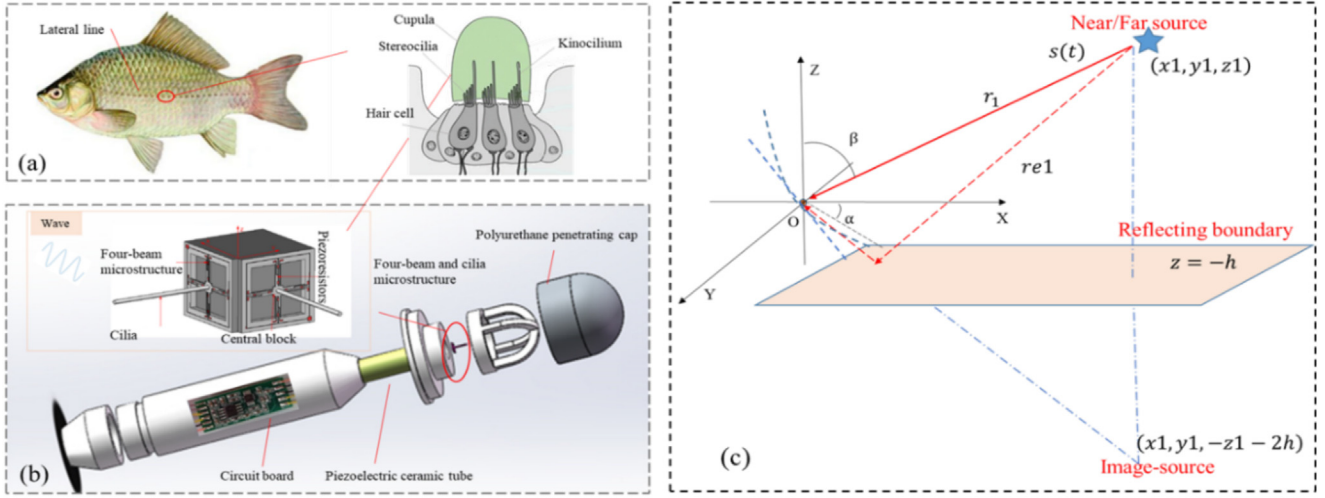


Fig. 1. Biomimetic microstructure of vector hydrophone and acoustic propagation model of reflection boundary.

and lower computational complexity [20]. However, all these algorithms are applicable when the sound source and hydrophone are not close to any boundary, and there is little research on the sound source or hydrophone being close to the reflection boundary [21–23].

In this article, we designed a fuzzy free positioning algorithm for MEMS vector hydrophones based on near and far field reflection boundaries. Firstly, different reflection models were established, and the array manifold matrix of angle and range parameters under double reflection was derived to illustrate the influence of reflection boundaries on azimuth estimation. Then, the orthogonal information of interference noise and signal in the MUSIC algorithm was utilized to solve the problem with reflection boundaries. The simulation and field experiment results show that the algorithm is feasible in the presence of far-field and near-field reflection boundaries. The simulation and experimental results demonstrate that the method is feasible in the presence of reflection boundaries.

2 The far/near reflect boundary model

2.1 The principle of azimuth estimation

The composite MEMS cilia hydrophone consists of a cilia biomimetic structure and piezoelectric ceramics. It can simultaneously measure X, Y, and Z three-dimensional vector information as well as sound pressure information, and cilia mimic the sound sensing mechanism of lateral organs in fish [24–26]. The three-dimensional microstructure and biomimetic principle of the vector hydrophone are shown in Figure 1a. The combination site of the cilia vector sensor is Figure 1b.

The signal reception model of MEMS vector hydrophone can be expressed as the following equation.

$$\begin{cases} P(t) = p(t) + n_p \\ v_x(t) = v(t)\cos\alpha\sin\beta + n_{vx} \\ v_y(t) = v(t)\sin\alpha\sin\beta + n_{vy} \\ v_z(t) = v(t)\cos\beta + n_{vz} \\ \frac{\partial v}{\partial t} = -\frac{1}{\rho}\nabla P \end{cases}, \quad (1)$$

where $P(t)$, $v_i(t)$ ($i = x, y, z$) represent the pressure signal and speed in 3D direction of MEMS vector hydrophone, respectively. And n_p , n_i ($i = vx, vy, vz$) represent the zero-mean uncorrelated Gaussian noise of four channels. The Eula equation reflects the physical relationship between sound pressure and vibration velocity.

2.2 Far/Near field source with reflecting boundary

In the three-dimensional Cartesian coordinate system, the spatial relationships between the sound source, vector hydrophone, and planar reflection boundary are shown in Figure 1c, and the hydrophone located at the coordinate origin. Without loss of generality, assuming that the reflection boundary is an infinitely large plane located at $z = -h$, where h is the vertical range of sensor and plane reflection boundary. Among them, $0 \leq \alpha \leq 2\pi$ represents the azimuth angle, and the pitching angle ($0 \leq \beta \leq \pi$) is the angle between target and z-direction.

Assuming that the source is isotropic point radiation source, the ideal radiation sound pressure signal is

$$P_{in}(r, t) = \frac{A}{r} e^{i[\omega t - k_{in} * r]}. \quad (2)$$

Among them, k_{in} is wavenumber vector, $k = \omega/c = |k_{in}| = |k_{re}|$. According to ray acoustics theory, an image source is generated by the acoustic source passing through the reflection plane. And the signals received by the vector hydrophone include direct wave $P_{in}(r, t)$ and reflected wave $P_{re}(r, t) = A/re * e^{i[\omega t - k_{re} * re]}$. When the sound wave is incident on the reflection boundary, the reflected wave will be incident on the hydrophone receiving end through the reflection angle. The complex coefficient $\mathcal{T}(r, \omega)$ represents the amplitude and phase variation of the reflected sound wave. It is related to the medium properties of sound propagation, acoustic signal frequency and reflection interface, as well as reflection angle.

$$\begin{aligned} P_{all}(r, t) &= P_{in}(r, t) + P_{re}(r, t) \\ &= \frac{A}{r} e^{i[\omega t - k_{in} * r]} + \mathcal{T}(r, \omega) \frac{A}{re} e^{i[\omega t - k_{re} * re]}. \end{aligned} \quad (3)$$

The physical propagation mechanism requires that the sound particles on both sides of the sound edge interface have the same velocity, that is, the propagation speed of the incident wave at the boundary is the same as that of the reflected wave. If hydrophone is in the far field of acoustic source, it can be approximated as a far-field plane wave. The acoustic impedance is $Z = \rho c$. When the hydrophone is in the near field of acoustic source, the distance cannot be ignored, and the received signal is a spherical wave. Acoustic impedance is a complex number $Z = \rho c \frac{ikr}{1+ikr}$. In this article, we assume that the incident sound wave is sinusoidal, and the vibration velocity can be expressed as

$$v = -\frac{1}{i\omega\rho} \nabla P = -\frac{1}{i\omega\rho} \frac{dP}{dr}. \tag{4}$$

According to equation (4), the vibration velocity signal in the X direction can be expressed as the derivative of sound pressure. Among them, the signals of mutually orthogonal Y and Z paths can be represented by a similar derivative process

See equation (5 below).

According to the relationship between scalar and vector sound fields, it can be inferred from formula (4) and (5) that the four channel signals of a vector hydrophone can be represented in the form of 4×1 vectors. Formula $a(\alpha, \beta, r)$ is also known as array flow pattern.

$$\begin{bmatrix} P \\ v_x \\ v_y \\ v_z \end{bmatrix} = \frac{Ae^{i\omega t}}{-ik\rho c} \times a(\alpha, \beta, r) = \frac{Ae^{i\omega t}}{-ik\rho c} \times \begin{bmatrix} a_p(\alpha, \beta, r) \\ a_x(\alpha, \beta, r) \\ a_y(\alpha, \beta, r) \\ a_z(\alpha, \beta, r) \end{bmatrix}. \tag{6}$$

2.3 Different reflecting boundary

In general, $\mathcal{T}(r, \omega) \in [-1, 1]$. And the following ideal cases can greatly simplify the situation.

The perfect reflection boundary: in this case, the incident wave enters an ideal rigid boundary that neither absorbs nor transmits any energy. At this point, $\mathcal{T}(r, \omega) = 1$.

The pressure release soft boundary: in this case, acoustic impedance of the input boundary is almost zero. The wave incident from the sea surface into the air can be approximated as a pressure release boundary problem. At this point, $\mathcal{T}(r, \omega) = -1$.

Away from the boundary (no boundary): $\mathcal{T}(r, \omega) = 0$. The sensor is located near the source, not close to any boundary. At this point, the receiving end is less affected by reflected waves and only considers direct waves.

Assuming the following two points hold true throughout the entire text:

- Acoustic source signal is a narrowband stationary signal that is statistically independent;
- Noise is white Gaussian noise that is statistically independent of the source signal.

3 Vector manifold matrix under reflection boundaries

The MUSIC algorithm is a spectrum peak search method based on feature subspace [18]. Since the vector hydrophone contains three vector channels and a scalar signal, a single vector hydrophone can obtain four feature subspaces. By utilizing the feature subspaces of the signal and noise, target orientation estimation can be achieved.

The output signal of the vector sensor is

$$\mathbf{X}(t) = \mathbf{a}_v(\alpha, \beta, r)\mathbf{s}(t) + \mathbf{n}(t) \tag{7}$$

where direction vector $\mathbf{a}_v(\alpha, \beta, r) = \mathbf{a}(\alpha, \beta, r) \otimes \mathbf{u}(\alpha, \beta, r)$, $\mathbf{n}(t)$ is the Gaussian noise. N is the number of elements in the array. Assuming $N=1$ here. The phase difference between three-dimensional vector signals is 0, assuming $\rho c = 1$. For the convenience of calculation and theoretical analysis, the acoustic impedance parameters are normalized, and the corresponding values can be replaced with

$$\begin{aligned} v_x &= \left(-\frac{1}{i\omega\rho} \frac{\partial P}{\partial r}\right)_x = \frac{1}{-i\omega\rho} \frac{\partial P_{all}(r, t)}{\partial x} \Big|_{r(x,y,z)=r_0(0,0,0)} = \frac{Ae^{i\omega t}}{-ik\rho c} \frac{\partial \left[\frac{e^{-ik*r}}{r} + \mathcal{T}(r, \omega) \frac{e^{-ik*re}}{re} \right]}{\partial x} \Big|_{r(x,y,z)=r_0(0,0,0)} \\ &= \frac{Ae^{i\omega t}}{-ik\rho c} \frac{\partial \left[\frac{e^{-ik*\sqrt{(x-x1)^2+(y-y1)^2+(z-z1)^2}}}{\sqrt{(y-y1)^2+(x-x1)^2+(z-z1)^2}} + \mathcal{T}(r, \omega) \frac{e^{-ik*\sqrt{(x-x1)^2+(y-y1)^2+(z+z1+2h)^2}}}{\sqrt{(y-y1)^2+(x-x1)^2+(z+z1+2h)^2}} \right]}{\partial x} \\ &= \frac{Ae^{i\omega t}}{-ik\rho c} \left[\frac{ik * e^{-ik*r} * x1 + e^{-ik*r} * \frac{x1}{r}}{r^2} + \frac{ik * e^{-ik*re} * \mathcal{T} * x1 + \frac{\partial \mathcal{T}(r, \omega)}{\partial x} \Big|_{r=r_0} * e^{-ik*re} * re + \mathcal{T} * e^{-ik*re} * \frac{x1}{re}}{re^2} \right] \\ &= \frac{Ae^{i\omega t}}{-ik\rho c} \left[\frac{ik + \frac{1}{r}}{r^2} * e^{-ik*r} * x1 + \frac{ik + \frac{1}{re}}{re^2} * e^{-ik*re} * \mathcal{T} * x1 + \frac{1}{re} * \frac{\partial \mathcal{T}(r, \omega)}{\partial x} \Big|_{r(x,y,z)=r_0(0,0,0)} * e^{-ik*re} \right] \end{aligned} \tag{5}$$

specific parameter information during actual calculation.

$$\mathbf{u} = \left[1, \frac{1 + \frac{1}{ikr}}{\rho c} \cos\alpha \sin\beta, \frac{1 + \frac{1}{ikr}}{\rho c} \sin\alpha \sin\beta, \frac{1 + \frac{1}{ikr}}{\rho c} \cos\beta \right]^T$$

$$\approx [1 \cos\alpha \sin\beta \sin\alpha \sin\beta \cos\beta]^T,$$

and $\mathbf{a}(\alpha, \beta, r)$ is

$$\mathbf{a}(\alpha, \beta, r) = \begin{bmatrix} 1 \\ e^{i\omega} \left[\begin{array}{c} -\frac{2\pi d}{\lambda} \cos\alpha \sin\beta \\ + \frac{\pi d^2}{\lambda r} (1 - (\cos\alpha \sin\beta)^2) \\ \vdots \\ -\frac{2\pi d(N-1)}{\lambda} \cos\alpha \sin\beta \\ + \frac{\pi d^2}{\lambda r} (N-1)^2 (1 - (\cos\alpha \sin\beta)^2) \end{array} \right] \\ e^{i\omega} \left[\begin{array}{c} -\frac{2\pi d(N-1)}{\lambda} \cos\alpha \sin\beta \\ + \frac{\pi d^2}{\lambda r} (N-1)^2 (1 - (\cos\alpha \sin\beta)^2) \end{array} \right] \end{bmatrix}. \quad (8)$$

Then, the covariance matrix of the array can be further resolved into

$$\mathbf{R} = \mathbf{E}(\mathbf{X}\mathbf{X}^H) = \mathbf{U}_S \sum_S \mathbf{U}_S^H + \mathbf{U}_N \sum_N \mathbf{U}_N^H. \quad (9)$$

where, \mathbf{U}_S , \mathbf{U}_N , \sum_S and \sum_N are the signal and noise eigenvectors, and the diagonal matrices of the signal and noise eigenvalues, respectively. \sum_S is a full rank matrix. Therefore, based on the subspace characteristics, noise subspace and the signal angle vector is orthogonal, that is

$$\mathbf{U}_N^H \mathbf{a}_v(\alpha, \beta, r) = 0. \quad (10)$$

Based on the characteristics of the feature subspace algorithm and feature matrix, the MUSIC spatial spectral function and array manifold can be expressed as the following equations

$$\mathbf{P}(\alpha, \beta, r) = \frac{1}{\mathbf{a}^H(\alpha, \beta, r) \mathbf{U}_N \mathbf{U}_N^H \mathbf{a}(\alpha, \beta, r)}. \quad (11)$$

See equation (12) below).

where $d = \frac{r}{1 + \frac{r}{\lambda}}$, $a = \frac{r}{r_e} e^{-i\frac{r}{\lambda}}$, $b = \left(\frac{r}{r_e}\right)^2 \frac{i\frac{r}{\lambda} + 1}{i\frac{r}{\lambda} - 1}$. Different reflection boundaries correspond to different reflection array manifolds.

3.1 Far field source with reflecting boundary

Due to the infinite range of the far-field, $r \rightarrow \infty$ can be substituted into formula (11). The far-field DOA can be found through one-dimensional spectral peaks. The MEMS vector hydrophone is in the acoustic source's far-field and near the reflecting boundary. And when $r \rightarrow \infty$, we can obtain that $\frac{r_e}{r} \rightarrow 1$, $\frac{h}{r} \rightarrow 0$, $r_e - r \rightarrow 2h \cos\beta$.

a. $\mathcal{T}(r, \omega) = 0$, without any reflecting boundary. The received signal array manifold can be simplified to

$$\mathbf{a}(\alpha, \beta, r) = \begin{bmatrix} -\rho c \\ \cos\alpha \sin\beta \\ \sin\alpha \sin\beta \\ \cos\beta \end{bmatrix}, \quad (13)$$

b. $\mathcal{T}(r, \omega) = 1$, vector hydrophone near a rigid reflecting boundary.

$$\mathbf{a}(\alpha, \beta, r) = \begin{bmatrix} -\rho c \frac{ikr}{1 + ikr} \left(1 + e^{-i2\frac{h}{\lambda} \cos\beta} \right) \\ \cos\alpha \sin\beta \left(1 + e^{-i2\frac{h}{\lambda} \cos\beta} \right) \\ \sin\alpha \sin\beta \left(1 + e^{-i2\frac{h}{\lambda} \cos\beta} \right) \\ \cos\beta \left(1 - e^{-i2\frac{h}{\lambda} \cos\beta} \right) \end{bmatrix}, \quad (14)$$

c. $\mathcal{T}(r, \omega) = -1$, vector hydrophone near a pressure release reflective soft boundary.

$$\mathbf{a}(\alpha, \beta, r) = \begin{bmatrix} -\rho c \frac{ikr}{1 + ikr} \left(1 - e^{-i2\frac{h}{\lambda} \cos\beta} \right) \\ \cos\alpha \sin\beta \left(1 - e^{-i2\frac{h}{\lambda} \cos\beta} \right) \\ \sin\alpha \sin\beta \left(1 - e^{-i2\frac{h}{\lambda} \cos\beta} \right) \\ \cos\beta \left(1 + e^{-i2\frac{h}{\lambda} \cos\beta} \right) \end{bmatrix}. \quad (15)$$

$$\mathbf{a}_v(\alpha, \beta, r) = \begin{bmatrix} a_p(\alpha, \beta, r) \\ a_x(\alpha, \beta, r) \\ a_y(\alpha, \beta, r) \\ a_z(\alpha, \beta, r) \end{bmatrix} = \begin{bmatrix} -\rho c d [1 + a * \mathcal{T}(r, \omega)] \\ \cos\alpha \sin\beta \left[1 + a * b * \mathcal{T}(r, \omega) + \frac{a * d}{ik} * \frac{\partial \mathcal{T}(r, \omega)}{\partial x} \Big|_{r=r_0} \right] \\ \sin\alpha \sin\beta \left[1 + a * b * \mathcal{T}(r, \omega) + \frac{a * d}{ik} * \frac{\partial \mathcal{T}(r, \omega)}{\partial y} \Big|_{r=r_0} \right] \\ \cos\beta \left[1 - a * b * \mathcal{T}(r, \omega) \right] + \frac{a * d}{ik} * \frac{\partial \mathcal{T}(r, \omega)}{\partial z} \Big|_{r=r_0} - \frac{2 * z_1}{r} * a * b * \mathcal{T}(r, \omega) \end{bmatrix} \quad (12)$$

Therefore, the array manifold is a function of elevation and azimuth angle, and the estimation of position is achieved through two one-dimensional searches.

3.2 Near field source with reflecting boundary

Due to the need to consider both angle and range in the near-field position parameters, its position information can be found through two first-order spatial spectral searches. According to the non-singularity of the subarray, the decomposition of the directional matrix can be achieved, and formula (8) can be expressed as (16)

$$\mathbf{a}(\alpha, \beta, r) = \zeta(\alpha, \beta)\eta(\alpha, \beta, r) = \begin{bmatrix} e^{j(-N)\frac{-2\pi d}{\lambda}\cos\alpha\sin\beta} & \dots & 0 \\ \vdots & \ddots & \vdots \\ 0 & \dots & 1 \\ \vdots & \ddots & \vdots \\ e^{j(N)\frac{-2\pi d}{\lambda}\cos\alpha\sin\beta} & \dots & 0 \\ e^{j(-N)^2\frac{\pi d^2}{\lambda r_i}(1 - (\cos\alpha\sin\beta)^2)} \\ \vdots \\ e^{j(-N+1)^2\frac{\pi d^2}{\lambda r_i}(1 - (\cos\alpha\sin\beta)^2)} \\ \vdots \\ 1 \end{bmatrix} * \begin{bmatrix} \\ \\ \\ \\ \\ \\ \\ \\ \\ \end{bmatrix}, \quad (16)$$

From the multiplication calculation rule of Kronecker, the equations (7) and (8) can be converted into

$$\mathbf{a}_r(\alpha, \beta, r) = [\zeta(\alpha, \beta)\eta(\alpha, \beta, r)] \otimes \mathbf{u}(r, \alpha, \beta) = [\zeta(\alpha, \beta) \otimes \mathbf{u}(r, \alpha, \beta)]\eta(\alpha, \beta, r) = v(\alpha, \beta)\eta(\alpha, \beta, r), \quad (17)$$

Regardless of the situation, $\eta(\alpha, \beta, r) \neq 0$. Therefore, DOA can be solved by the following equation.

$$gg(\alpha, \beta) = v^H(\alpha, \beta)U_N U_N^H v(\alpha, \beta) = 0 \quad (18)$$

The satisfaction of singular conditions in matrices is a sufficient and necessary condition for equation (18) to hold. Only the true DOA satisfies the rank reduction condition. Substitute DOA into the spectrum function (19) for range search.

$$\mathbf{P}(r) = \frac{1}{\mathbf{a}^H(r)U_N U_N^H \mathbf{a}(r)}. \quad (19)$$

When the vector hydrophone is located near the near-field and reflection boundary, different reflection boundaries correspond to different array manifold matrices. The array manifold of MUSIC algorithm under different reflection coefficients can be represented as follows:

a. $\mathcal{T}(r, \omega) = 0$, without any reflecting boundary.

$$\mathbf{a}(\alpha, \beta, r) = \begin{bmatrix} -\rho c \frac{ikr}{1 + ikr} \\ \cos\alpha\sin\beta \\ \sin\alpha\sin\beta \\ \cos\beta \end{bmatrix}. \quad (20)$$

b. $\mathcal{T}(r, \omega) = 1$, sensor near a rigid reflecting boundary.

See equation (21) below.

c. $\mathcal{T}(r, \omega) = -1$, vector hydrophone near a pressure release reflecting soft boundary.

See equation (22) is next page).

$$\mathbf{a}(\alpha, \beta, r) = \begin{bmatrix} -\rho c \frac{i\frac{r}{\lambda}}{1 + i\frac{r}{\lambda}} \left[1 + \frac{r}{re} e^{-i\frac{re-r}{\lambda}} \right] \\ \cos\alpha\sin\beta \left[1 + \frac{r}{re} e^{-i\frac{re-r}{\lambda}} * \left(\frac{r}{re}\right)^2 \frac{i\frac{re}{\lambda} + 1}{i\frac{r}{\lambda} + 1} \right] \\ \sin\alpha\sin\beta \left[1 + \frac{r}{re} e^{-i\frac{re-r}{\lambda}} * \left(\frac{r}{re}\right)^2 \frac{i\frac{re}{\lambda} + 1}{1 + i\frac{r}{\lambda}} \right] \\ \cos\beta \left[1 - \frac{r}{re} e^{-i\frac{re-r}{\lambda}} * \left(\frac{r}{re}\right)^2 \frac{1 + i\frac{re}{\lambda}}{i\frac{r}{\lambda} + 1} \right] - 2 * \frac{r}{re} e^{-i\frac{re-r}{\lambda}} * \left(\frac{r}{re}\right)^2 \frac{i\frac{re}{\lambda} + 1}{i\frac{r}{\lambda} + 1} * \frac{h}{r} \end{bmatrix} \quad (21)$$

$$a(\alpha, \beta, r) = \begin{bmatrix} -\rho c \frac{i \frac{r}{\lambda}}{1 + i \frac{r}{\lambda}} \left[1 - \frac{r}{re} e^{-i \frac{re-r}{\lambda}} \right] \\ \cos \alpha \sin \beta \left[1 - \frac{r}{re} e^{-i \frac{re-r}{\lambda}} * \left(\frac{r}{re} \right)^2 \frac{i \frac{re}{\lambda} + 1}{i \frac{r}{\lambda} + 1} \right] \\ \sin \alpha \sin \beta \left[1 - \frac{r}{re} e^{-i \frac{re-r}{\lambda}} * \left(\frac{r}{re} \right)^2 \frac{i \frac{re}{\lambda} + 1}{i \frac{r}{\lambda} + 1} \right] \\ \cos \beta \left[1 + \frac{r}{re} e^{-i \frac{re-r}{\lambda}} * \left(\frac{r}{re} \right)^2 \frac{1 + i \frac{re}{\lambda}}{i \frac{r}{\lambda} + 1} \right] + 2 * \frac{r}{re} e^{-i \frac{re-r}{\lambda}} * \left(\frac{r}{re} \right)^2 \frac{1 + i \frac{re}{\lambda}}{i \frac{r}{\lambda} + 1} * \frac{h}{r} \end{bmatrix} \quad (22)$$

In summary, the array manifold of near-field sources is a function of azimuth, elevation, and distance. Based on peak search, it is possible to estimate the range and DOA of acoustic source.

3.3 Double reflecting boundary

When there is a double reflection boundary, the received signal includes a direct wave $P_{in}(r, t)$ and two reflected waves $P_{re1}(r, t), P_{re2}(r, t)$, and the hydrophone and planar reflection boundary models are shown in Figure 2a. Assuming the reflection boundary is located at $z_1 = -h_1, z_2 = h_2$. $\mathcal{T}_1(r, \omega), \mathcal{T}_2(r, \omega)$ are the complex reflection coefficients of the water-air surface boundary and the underwater boundary layer, respectively. So, the received signal can be represented as

$$P_{all}(r, t) = P_{in} + P_{re1} + P_{re2} = \frac{A}{r} e^{i[\omega t - k_{in} * r]} + \mathcal{T}_1(r, \omega) \frac{A}{re1} e^{i[\omega t - k_{re1} * re1]} + \mathcal{T}_2(r, \omega) \frac{A}{re2} e^{i[\omega t - k_{re2} * re2]}. \quad (23)$$

Then, formula (12) takes derivatives for X, Y, and Z to obtain the physical values of the three vector vibration velocity channels, and substitutes the coordinates into the formula. At this point, the manifold matrix of the target can be simplified as

See equation (24) below.

$$a(\alpha, \beta, r) = \begin{bmatrix} -\rho c d [1 + a1 * \mathcal{T}_1(r0, \omega) + a2 * \mathcal{T}_2(r0, \omega)] \\ \cos \alpha \sin \beta \left[1 + a1 * b1 * \mathcal{T}_1(r0, \omega) + a2 * b2 * \mathcal{T}_2(r0, \omega) + \frac{a1 * d}{ik} * \frac{\partial \mathcal{T}_1(r, \omega)}{\partial x} \Big|_{r=r0} + \frac{a2 * d}{ik} * \frac{\partial \mathcal{T}_2(r, \omega)}{\partial x} \Big|_{r=r0} \right] \\ \sin \alpha \sin \beta \left[1 + a1 * b1 * \mathcal{T}_1(r0, \omega) + a2 * b2 * \mathcal{T}_2(r0, \omega) + \frac{a1 * d}{ik} * \frac{\partial \mathcal{T}_1(r, \omega)}{\partial y} \Big|_{r=r0} + \frac{a2 * d}{ik} * \frac{\partial \mathcal{T}_2(r, \omega)}{\partial y} \Big|_{r=r0} \right] \\ \cos \beta \left[1 - a1 * b1 * \mathcal{T}_1(r0, \omega) - a2 * b2 * \mathcal{T}_2(r0, \omega) \right] + \frac{a1 * d}{ik} * \frac{\partial \mathcal{T}_1(r, \omega)}{\partial z} \Big|_{r=r0} + \frac{a2 * d}{ik} * \frac{\partial \mathcal{T}_2(r, \omega)}{\partial z} \Big|_{r=r0} - m \end{bmatrix}. \quad (24)$$

where

$$d = \frac{i \frac{r}{\lambda}}{1 + i \frac{r}{\lambda}}, a1 = \frac{re^{-i \frac{re1-r}{\lambda}}}{re1}, a2 = \frac{re^{-i \frac{re2-r}{\lambda}}}{re2}, \\ b1 = \left(\frac{r}{re1} \right)^2 \frac{i \frac{re1}{\lambda} + 1}{i \frac{r}{\lambda} + 1}, b2 = \left(\frac{r}{re2} \right)^2 \frac{i \frac{re2}{\lambda} + 1}{i \frac{r}{\lambda} + 1}, \\ m = \frac{2h1}{r} a1 * b1 * \mathcal{T}_1(r0, \omega) + \frac{2h2}{r} a2 * b2 * \mathcal{T}_2(r0, \omega).$$

4 Simulation of far/near source localization with different reflection boundaries

This section verifies the performance of the proposed algorithm in the case of reflection boundaries through simulation experiments. Without loss of generality, the localization of vector hydrophones with different reflection boundaries is considered. Assuming the signal is a single frequency signal. In addition, symbol RMSE and SNR represent the root mean square error and received signal-to-noise ratio, respectively [27]. Measure the performance of the proposed algorithm through 500 independent Monte Carlo repeated experiments and compare it with the corresponding CRB.

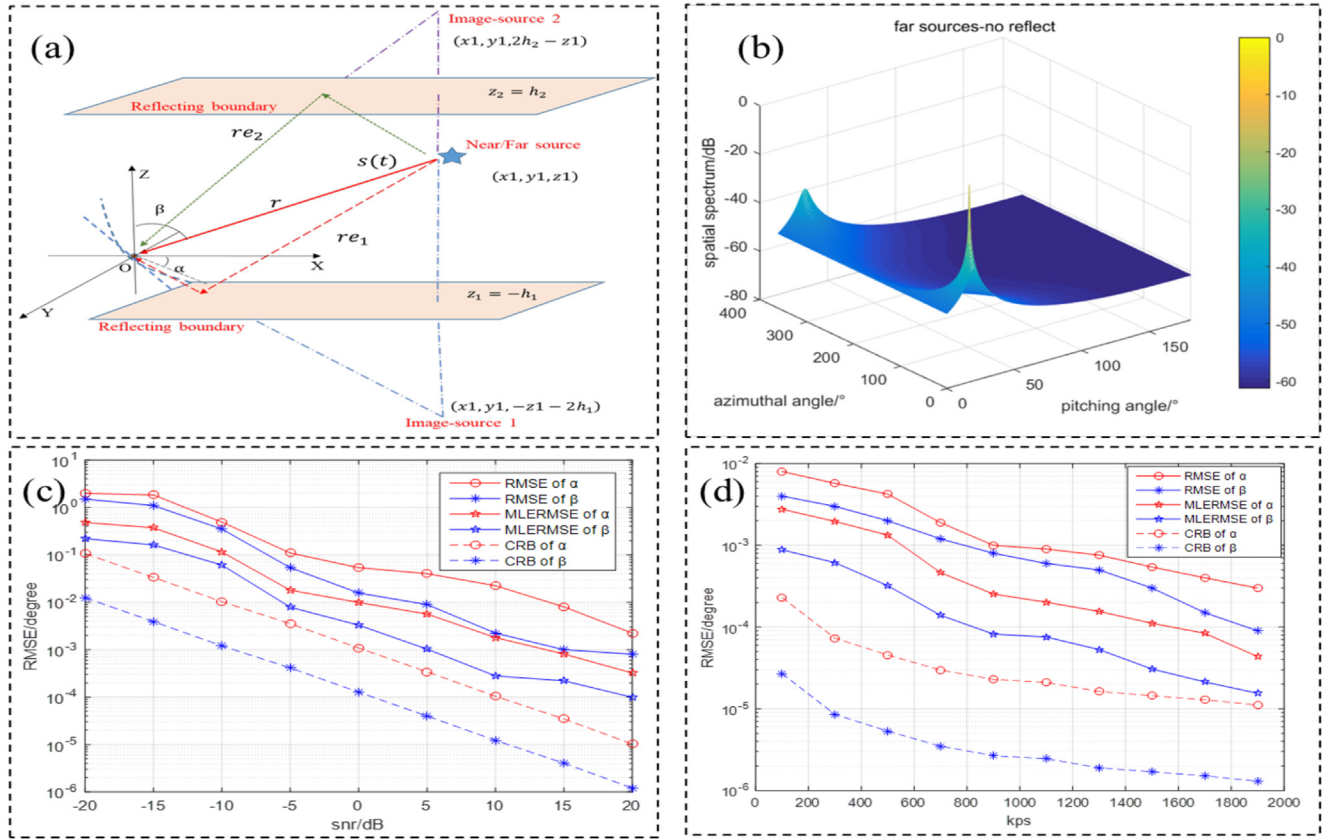


Fig. 2. (a) The double reflecting boundary modal. (b) The DOA of far field sources. (c) Comparison results of range estimation. (d) Comparison results of DOA estimation.

4.1 Direction estimation under far-field source with reflecting boundary

In this section, the proposed algorithm is used to locate far-field sources with different reflection boundaries. Assuming the existence of a far-field source: $\{\alpha=10^\circ, \beta=20^\circ, z=-0.5\lambda\}$. Firstly, assuming the number of snapshots (NS) is 1000 and SNR is 20 dB. The results indicate that the vector hydrophone achieves non fuzzy orientation within the $[0:2 * \pi]$ angle. Next, we will mainly study and discuss several special reflection situations.

a. When $\mathcal{T}(r, \omega) = 0$, the hydrophone is located in the far-field and not close to any boundaries. At this point, there is no reflected wave (i.e. $P_{re}(r, t) = 0$).

Firstly, assuming SNR is 20 dB and NS is 1000. The proposed algorithm calculates the azimuth and elevation angles as shown in Figure 2b. Secondly, NS is 1000, and SNR varies uniformly from -15 dB to 20 dB. Figure 2c shows a negative correlation between angle error and SNR. Thirdly, assuming SNR is 20 dB and NS increases from 100 to 2000. Figure 2d shows that DOA estimation error is also negatively correlated with NS. Finally, through 500 repeated Monte Carlo experiments, this conclusion was further validated by comparing it with the maximum likelihood estimation algorithm and CRB results.

b. When $\mathcal{T}(r, \omega) = 1$, the vector hydrophone is in the far-field, close to the rigid boundary. At this point, there is a reflected wave (i.e. $P_{re}(r, t) = \frac{A}{r_e} e^{i[\omega t - k_{re} * r_e]}$). The MUSIC algorithm calculates the far-field azimuth and elevation parameters as shown in Figure 3a. The corresponding simulation results are shown in Figures 3b and 3c.

c. When $\mathcal{T}(r, \omega) = -1$, the vector hydrophone is in the far field, close to the pressure release boundary. At this point, there is a reflected wave (i.e. $P_{re}(r, t) = -\frac{A}{r_e} e^{i[\omega t - k_{re} * r_e]}$).

In this reflection scenario, the simulation conditions are the same as for parts a and b. Calculate the spatial azimuth parameters of the distant source using the MUSIC method, such as Figure 3d. The simulation results of DOA parameters with changes in SNR and NS are shown in Figures 3e and 3f javascript;. DOA estimation error is negatively correlated with NS and SNR. Meanwhile, the angular resolution of DOA under pressure release boundary is lower than that without reflection boundary and rigid reflection boundary.

4.2 Direction estimation under near-field source with reflecting boundary

In this section, the proposed method achieves the near source DOA and range parameter estimation with different reflecting boundary. Assuming that $z = -0.5\lambda$. Using the

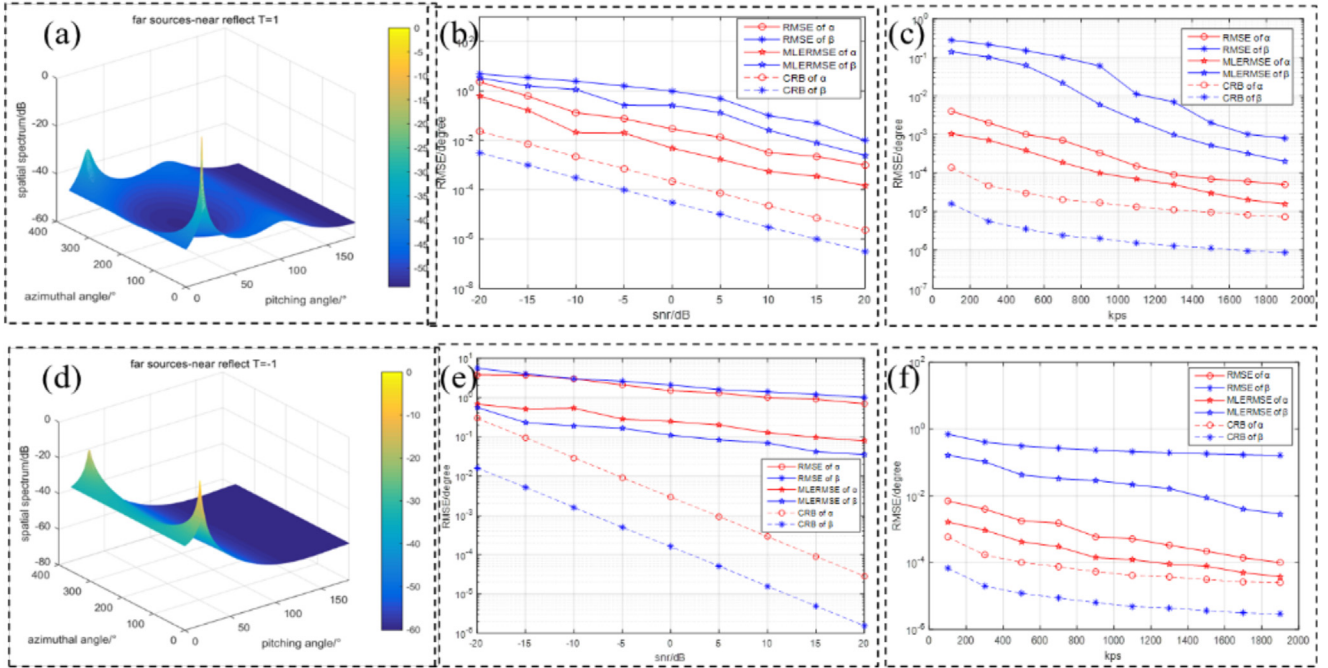


Fig. 3. (a) The DOA of far field sources when $\mathcal{T}(r, \omega) = 1$. (b) SNR and DOA RMSE. (c) NS and DOA RMSE. (d) The DOA of far field sources when $\mathcal{T}(r, \omega) = -1$. (e) SNR and DOA RMSE. (f) NS and DOA RMSE.

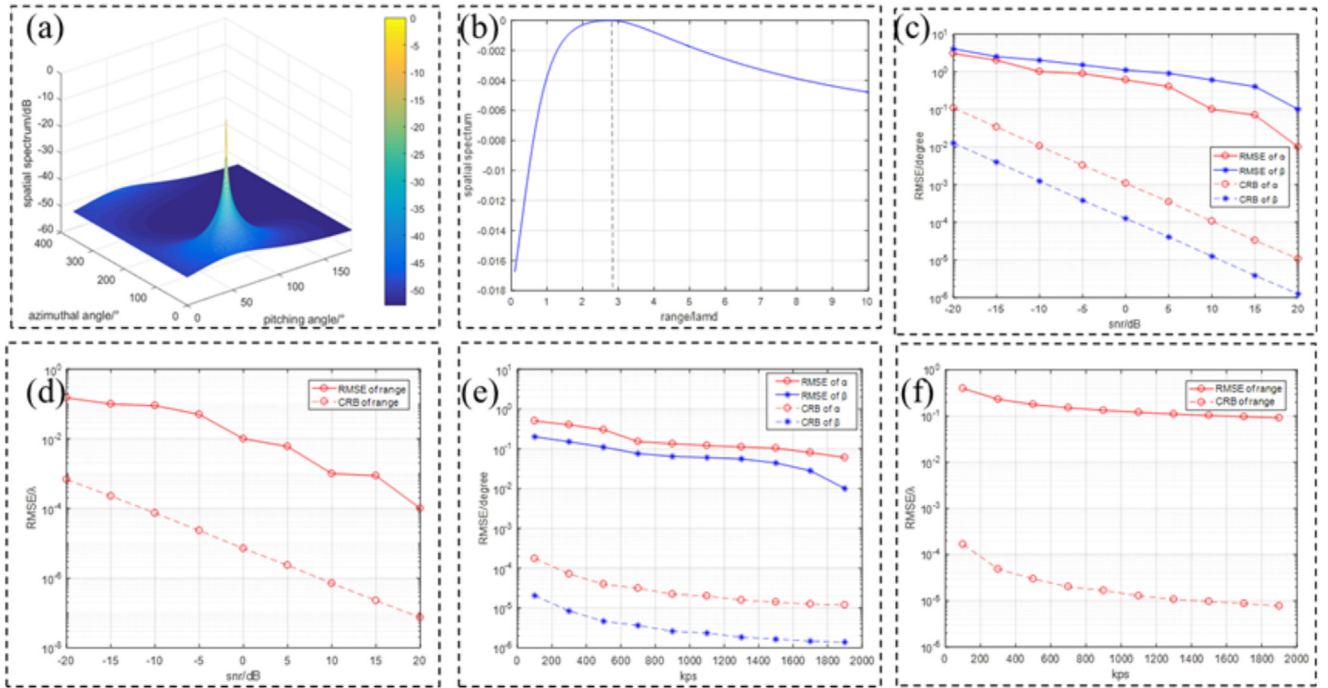


Fig. 4. (a) The DOA of near-field sources. (b) The range of near-field sources. (c) SNR and DOA RMSE. (d) SNR and range RMSE. (e) NS and DOA RMSE. (f) NS and range RMSE.

array manifolds of section 3.2 to calculate the DOA and range parameters. Next, we mainly study and discuss the localization under several special reflecting boundary cases.

a. When $\mathcal{T}(r, \omega) = 0$, that is, the sensor is not close to any boundary. In such a sound field environment, there will be no reflected waves (i.e. $P_{re}(r, t) = 0$). Assuming that the near field source is: $\{\alpha = 50^\circ, \beta = 60^\circ, r = 3\lambda\}$.

As previously mentioned, assuming SNR is 20 dB and NS is 1000. The proposed algorithm calculates the azimuth; elevation angles and range are shown in Figures 4a and 4b. Secondly, NS is 1000, and SNR varies uniformly from -15 dB to 20 dB. Figure 4c shows a negative correlation between angle error and SNR. Figure 4d shows a negative correlation between range error and SNR. Thirdly,

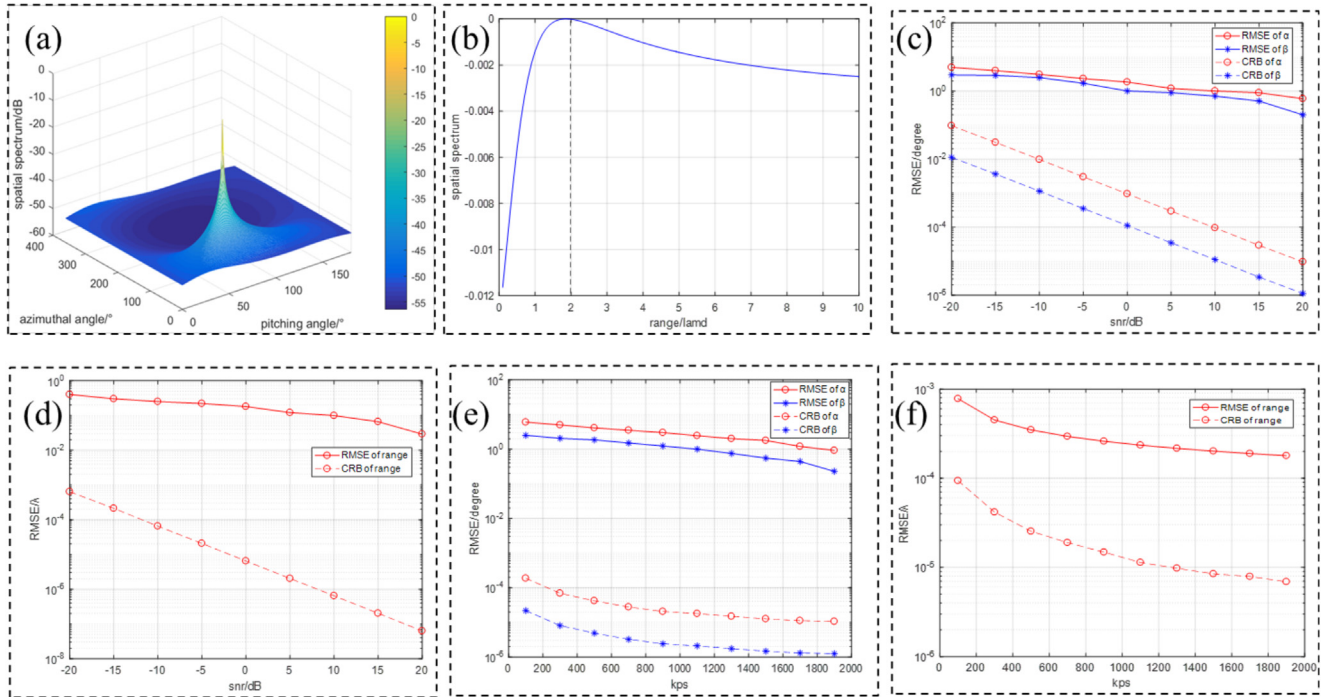


Fig. 5. (a) DOA. (b) range. (c) SNR and DOA RMSE. (d) SNR and range RMSE. (e) NS and DOA RMSE. (f) NS and range RMSE.

assuming SNR is 20 dB and NS increases from 100 to 2000. Figures 4e and 4f shows that DOA and range error are also negatively correlated with NS. Finally, the conclusion was further validated through 500 repeated Monte Carlo experiments.

b. When $\mathcal{T}(r, \omega) = 1$, that is, sensor is located in the near-field and near a rigid boundary. In such a sound field environment, there will be one reflected wave in the propagation model of Figure 2 (i.e. $P_{re}(r, t) = \frac{A}{r_e} e^{i[\omega*t - k_{re}*r_e]}$). Assuming that the near field source is: $\{\alpha = 50^\circ, \beta = 60^\circ, r = 2\lambda\}$.

In the case of rigid reflecting boundary $\mathcal{T}(r, \omega) = 1$, similar to the process of module A, the corresponding simulation results are shown in the Figures 5a and 5b. Figures 5c and 5d show the comparison results of SNR and NS on DOA and distance estimation, respectively. The results of CRB are also shown in Figure 5.

c. When $\mathcal{T}(r, \omega) = -1$, that is, the sensor is near a pressure release soft boundary. In such a sound field environment, there will be one reflected wave in the propagation model of Figure 2 (i.e. $P_{re}(r, t) = -\frac{A}{r_e} e^{i[\omega*t - k_{re}*r_e]}$). Assuming that the near field source is: $\{\alpha = 50^\circ, \beta = 60^\circ, r = \lambda\}$.

The simulation conditions are the same as part a. According to the vector MUSIC algorithm, we can obtain the angle and range parameter values of source, as shown in Figures 6a and 6b. Figures 6c–6f respectively show the relationship between SNR, NS and DOA, range. At the same time, the angle resolution of DOA estimation under pressure release boundary is lower than the case without reflecting boundary and rigid reflecting boundary.

4.3 Double reflecting boundary case

In this section, the proposed method achieves near and far field sources with double reflection boundaries. Assuming that the parameter of sources are: $\{\alpha = 20^\circ, \beta = 70^\circ, r = 1.5\lambda\}$, $\{\alpha = 30^\circ, \alpha = 45^\circ, r \rightarrow \infty\}$. The two reflection boundaries are rigid reflection boundary and pressure release boundary, namely $\mathcal{T}_1(r, \omega) = 1, \mathcal{T}_2(r, \omega) = -1$. The reflective boundary is an infinitely large two-dimensional Cartesian plane parallel to the z-axis, with coordinates $z_1 = -0.5\lambda, z_2 = 2\lambda$.

We assume the SNR is 20 dB and NS is 1000. Figures 7a and 7b show the angle and distance results of near-field source with double reflection boundaries. Figure 7c shows the far field DOA results with double reflection boundaries. The results indicate that vector sensor can fulfil non fuzzy positioning under double reflection boundary conditions. The specific array manifold relationship provides a foundation for azimuth estimation experiments in real field environments.

5 Experimental testing of reflection boundary localization

In order to further verify vector localization in complex environments, field experiments were conducted at Fenhe Reservoir ii. The hydrological conditions at the experimental site are wide, and the depth of over 20 meters.

The experimental water area is wide with an average depth of about 20 meters. The fish lip transducer and hydrophone are used for transmitting and receiving sound

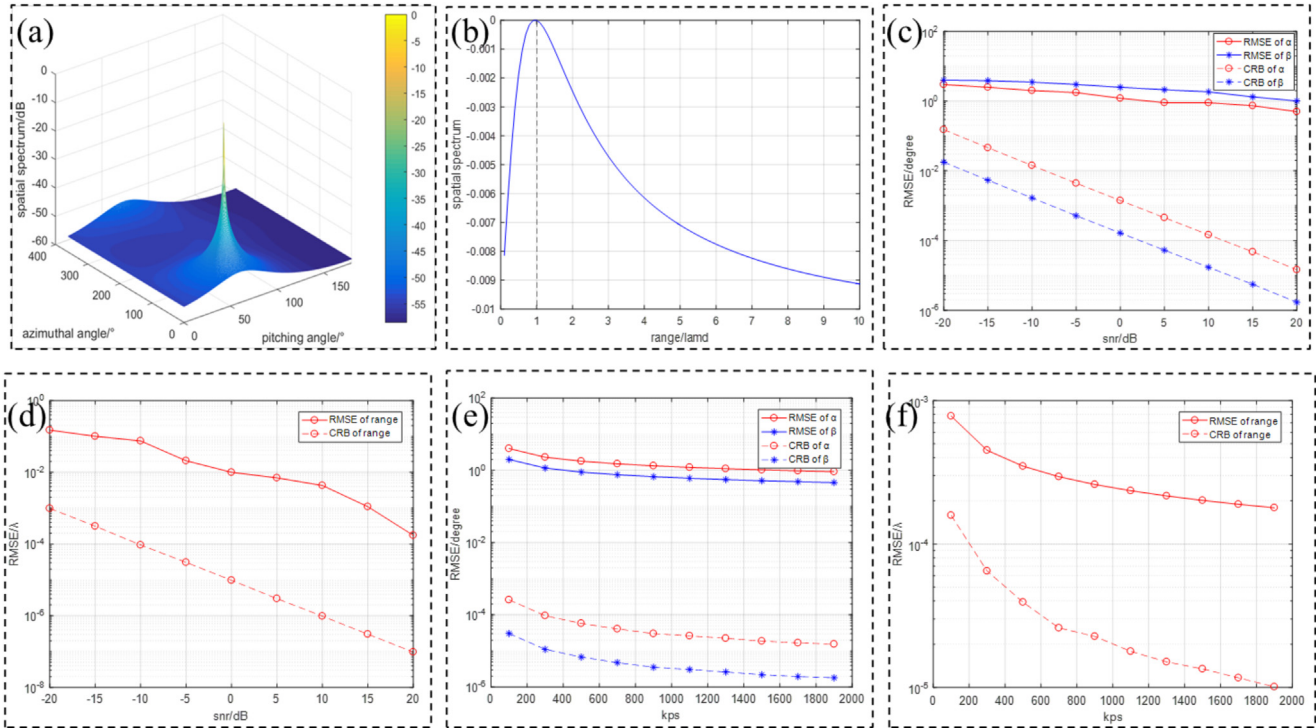


Fig. 6. (a) DOA. (b) range. (c) SNR and DOA RMSE. (d) SNR and range RMSE. (e) NS and DOA RMSE. (f) NS and range RMSE.

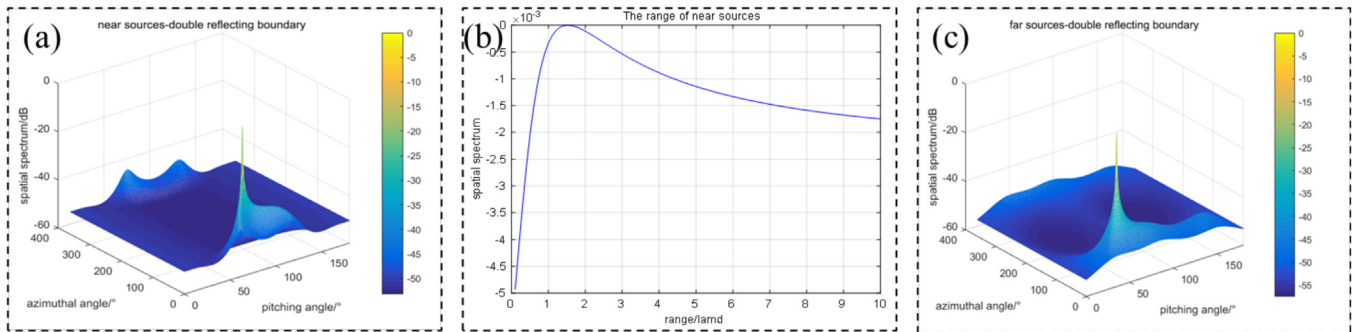


Fig. 7. Double reflecting boundary. (a) near field DOA. (b) near field range. (c) far field DOA.

signals, respectively. And the NI acquisition card collects the sound signals. The outdoor experimental conditions are shown in Figure 8, mainly includes water surface and underwater reflection.

Using GPS and compass to calibrate position data, the speedboat is placed in the water from the side of the speedboat, with the transmitting transducer placed in the direction of the hydrophone at approximately 33 degrees. The transmitted signal is a 630 Hz pulse signal located approximately 100 meters away. The received signal and processed result are shown in Figures 9a and 9b, achieving vector localization detection under reflection conditions. According to the vector algorithm calculation results, the error is within 5 degrees, indicating that the method is feasible. In the future, more complex work verification will be conducted, and this research has important guiding significance.

6 Conclusion

In this paper, the fuzzy free localization method for vector hydrophones under far and near reflection boundary conditions is proposed. The combination of vector information of sound field and orthogonal rank reduction algorithm solves the problem of fuzzy positioning. Firstly, several measurement models suitable for different sound fields and reflection conditions were established, and the array manifold matrix of the DOA angle and distance of the sound source under dual reflection was derived. Then compare the simulation results with CRB and maximum likelihood estimation algorithms to further validate the efficiency of the algorithm. This method not only solves the problem of ambiguity between the left and right sides, but also achieves high-precision angle and distance estimation

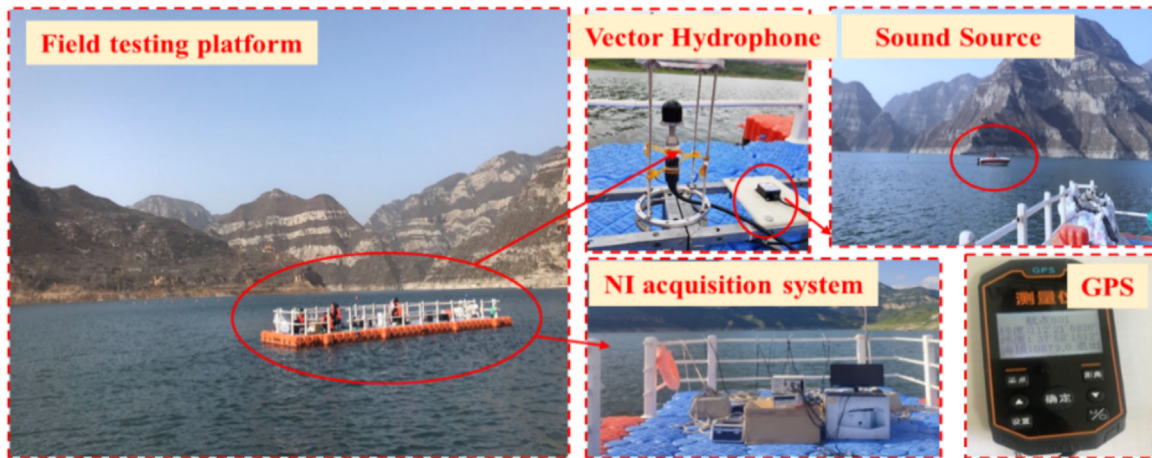


Fig. 8. The experimental site.

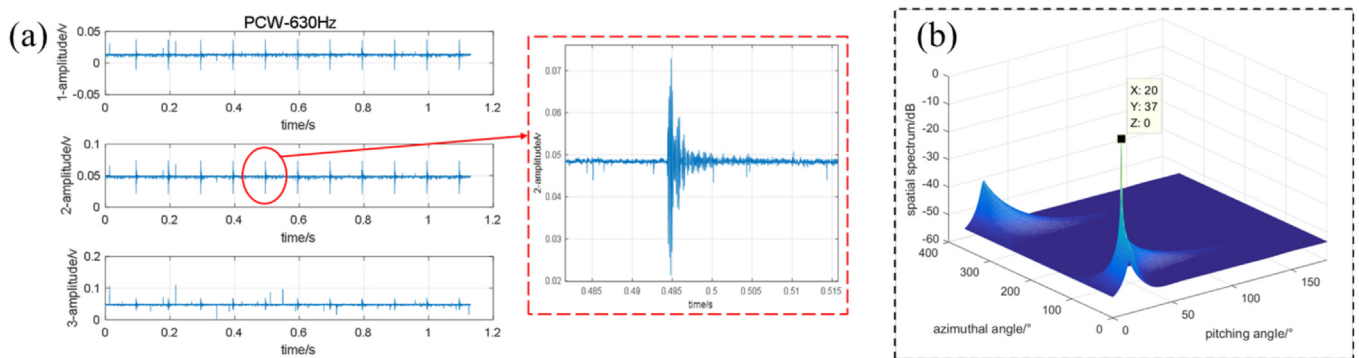


Fig. 9. (a) Received 630 Hz pulse signal. (b) Localization results of external field reflection algorithm

in special situations. This study has promoted the exploration of hydrophones and underwater acoustic engineering.

Funding

This work was supported by The Natural Youth Science Foundation of Shanxi province (202203021212015). Science and Technology Innovation Plan for colleges and universities in Shanxi Province (2022L575), Taiyuan University Scientific Research Projects (24TYQB09, 24TYZD02, 24TYZD04).

Conflicts of interest

The authors have no conflicts to disclose.

Data availability statement

The data that support the findings of this study are available from the corresponding author upon reasonable request.

Author contribution statement

Zhenzhen Shang: Conceptualization (equal); Methodology (equal); Software (equal); Supervision (equal); Writing – original

draft (equal). Xiaoyong Zhang: Visualization (equal). Hairong Kou: Writing – review & editing (equal). Libo Yang: Investigation (equal). Guojun Zhang: Data curation (equal).

References

1. Compiled by the Chinese physical society hydroacoustics (Science Press, 1962)
2. C.B. Leslie, Development of a velocity hydrophone, The Journal of the Acoustical Society of America, 28, 711–715. (1956)
3. L. Liu, W. Zhang et al., Package optimization of the cilium-type MEMS bionic vector hydrophone, IEEE Sens. J. 14, 1185–1192 (2014)
4. C. Xue, S. Chen et al., Design, fabrication, and preliminary characterization of a novel MEMS bionic vector hydrophone, Microelectron. J. 38, 1021–1026 (2007)
5. P. Felisberto, J. Schneiderwind, Comparing the resolution of Bartlett and MVDR estimators for bottom parameter estimation using pressure and vector sensor short array data (IEEE/MTS Oceans, 2012)
6. K.G. Nagananda, G.V. Anand, Subspace intersection method of high-resolution bearing estimation in shallow ocean using acoustic vector sensors, Signal Process. 90, 105–118 (2010)

7. D. Levin, E.A.P. Habets, On the angular error of intensity vector based direction of arrival estimation in reverberant sound fields, *J. Acoust. Soc. Am.* 128, 1800–1811 (2010)
8. Z. Shang, W. Zhang, A study on MEMS vector hydrophone and its orientation algorithm, *Sens. Rev.* 40, 191–201 (2020)
9. M. Hawkes, A. Nehorai, Acoustic vector-sensor processing in the presence of a reflecting boundary, *IEEE Trans. Signal Process.* 48, 2981–2993 (2000)
10. H. Keshavarz, Beam patterns of an underwater acoustic vector hydrophone located near a reflecting boundary (*Oceans IEEE*, 2012)
11. M. Hawkes, A. Nehorai, Acoustic vector-sensor processing in the presence of a reflecting boundary, *IEEE Trans. Signal Process.* 48, 2981–2993 (2000)
12. Y. Cho, M.J. Roan, Adaptive near-field beamforming techniques for sound source imaging, *J. Acoust. Soc. Am.* 125, 944–957 (2009)
13. Y. Wu, K.T. Wong, Near-field/far-field array manifold of an acoustic vector-sensor near a reflecting boundary, *J. Acoust. Soc. Am.* 139, 3159–3176 (2016)
14. P.K. Tam, K.T. Wong, Cramr-Rao bounds for direction finding by an acoustic vector sensor under nonideal gain-phase responses, noncollocation, or nonorthogonal orientation, *IEEE Sens. J.* 9, 969–982 (2009)
15. K.T. Wong, M.D. Zoltowski, Polarization-beamspace self-initiating MUSIC for azimuth/elevation angle estimation (*Radar IET*, 1997)
16. P. Jian, L. Zhang et al., Analytical models for electroosmotic consolidation of layered soil systems considering the boundary effects of horizontal electrodes, *Int. J. Numer. Anal. Methods Geomech.* 48 (2024)
17. H. Ma, H. Tao, Three-dimensional mixed far-field and near-field sources localization utilizing cross tripole array, *Circuits Syst. Signal Process.: CSSP*, 42, 4320–4342 (2023)
18. Z. Zheng, M. Fu et al., Mixed far-field and near-field source localization based on subarray cross-cumulant, *Signal Process.* 150, 51–56 (2018)
19. Y. Wu, W. Wang et al., Asymptotic properties of kernel density and hazard rate function estimators with censored widely orthant dependent data, *Comput. Stat.* (2025)
20. Z. Shang, Dimension reduction localization algorithm of mixed sources based on MEMS vector hydrophone array. *Micromachines* 13, 626 (2022)
21. J. Yuan, X. Meng, Manipulation of acoustic wave reflection for arbitrary reflecting surfaces based on acoustic meta surfaces, *Int. J. Modern Phys. B. Condensed Matter Phys. Stat. Phys. Appl. Phys.* 36 (2022)
22. J. Zhang, Y. Qu et al., Acoustic waves radiated from two degrees-of-freedom nonlinear rigid oscillator systems immersed in unbounded compressible fluid, *J. Vib. Acoust.: Trans. ASME*, 144 (2022)
23. C. Dailey, N. Afshordi, Reflecting boundary conditions in numerical relativity as a model for black hole echoes, (2023)
24. E.S. Hassan, Mathematical analysis of the stimulus for the lateral line organ, *Biol. Cybern.* 52, 23–36 (1985)
25. G. Zhang, P. Wang et al., Improvement of the MEMS bionic vector hydrophone, *Microelectron. J.* 42, 815–819 (2011)
26. N. Guo, G. Zhang, Combined MEMS 3D vector acoustic sensors, *Micronanoelectron. Technol.* (2015)
27. S. Kamal, M. Supriya, Blind source separation of nonlinearly mixed ocean acoustic signals using slow feature analysis (*Ocean IEEE*, 2011)

Cite this article as: Zhenzhen Shang, Xiaoyong Zhang, Hairong Kou, Libo Yang, Guojun Zhang, Research on the direction estimation algorithm of vector hydrophones under near-field and far-field reflecting boundary, *Int. J. Metrol. Qual. Eng.* 17, 3 (2026), <https://doi.org/10.1051/ijmqe/2025012>